Excitonic fine structure splitting in type-II quantum dots

V. Křápek*
Central European Institute of Technology, Brno University of Technology, Technická 10, 616 00 Brno, Czech Republic

P. Klenovský
Institute of Condensed Matter Physics, Masaryk University, Kotlářská 2, 611 37 Brno, Czech Republic
and Central European Institute of Technology, Masaryk University, Kamenice 753, 625 00 Brno, Czech Republic

T. Šikola
Central European Institute of Technology, Brno University of Technology, Technická 10, 616 00 Brno, Czech Republic
and Institute of Physical Engineering, Brno University of Technology, Technická 2, 616 69 Brno, Czech Republic
(Received 30 April 2015; revised manuscript received 9 September 2015; published 25 November 2015)

Excitonic fine structure splitting in quantum dots is closely related to the lateral shape of the wave functions. We have studied theoretically the fine structure splitting in InAs quantum dots with a type-II confinement imposed by a GaAsSb capping layer. We show that very small values of the fine structure splitting comparable with the natural linewidth of the excitonic transitions are achievable for realistic quantum dots despite the structural elongation and the piezoelectric field. For example, varying the capping layer thickness allows for a fine tuning of the splitting energy. The effect is explained by a strong sensitivity of the hole wave function to the quantum dot structure and a mutual compensation of the electron and hole anisotropies. The oscillator strength of the excitonic transitions in the studied quantum dots is comparable to those with a type-I confinement which makes the dots attractive for quantum communication technology as emitters of polarization-entangled photon pairs.

DOI: 10.1103/PhysRevB.92.195430 PACS number(s): 71.35.−y, 73.21.La, 81.05.Ea

I. INTRODUCTION

Excitonic fine structure splitting (FSS) is a tiny energy splitting of two bright exciton states confined in quantum dot (QD) heterostructures with a typical magnitude ranging from units to hundreds μeV. It is manifested in a doublet structure of the exciton recombination band. It was observed for the first time in GaAs/AlGaAs quantum wells with fluctuating thickness [1] and then in various QD systems [2–5]. Soon after its discovery it was attributed to the electron-hole exchange interaction [6] and its finite value was related to the reduced symmetry, which needs to be lower than D_{2d} [2].

The interest in FSS is triggered by both fundamental and application points of view. FSS helps to distinguish the spectral features originating in the recombination of exciton (doublet), biexciton (doublet with opposite polarization-energy dependence), and trion (singlet) [2,7,8]. It plays an important role in the spin initialization, e.g., in electron spin memories [9] or in exciton dynamics and dephasing [10–13]. It provides some insight into the size and shape of QDs [14,15]. Benson's proposal of the source of entangled photon pairs relying on zero FSS [16] has called for the preparation of QD systems with low FSS. Using (111) substrates for the growth of InAs QDs reduced both structural asymmetry and piezoelectric contribution [17]. Another attempt involved strain-free GaAs/AlGaAs QDs with zero piezoelectric field, which, however, still exhibited a finite FSS due to structural elongation [5,18]. Postgrowth annealing of InAs QDs allowed one to decrease FSS from 96 μeV to a mere 6 μeV [19] or even to invert the bright exciton levels with the minimum FSS value of 4 μeV [20] (which might be underestimated, though, as the rotation of the polarization upon the levels anticrossing was disregarded). Another class of approaches is based on in-operation tuning, where the originally large value of FSS is reduced by applying the external field: electric [21,22], magnetic [2,23], or strain. The external strain field allowed one to reach FSS below experimental resolution in GaAs/AlGaAs QDs [24,25]; the simultaneous application of electric field allowed for a more powerful symmetry restoration and rather universal recovery of low FSS [26]. The experimental generation of polarization-entangled photon pairs in low-FSS QDs has been reported [27–31]. FSS has also been studied in QDs emitting at infrared telecommunication wavelengths [32–36].

Various effects contributing to the FSS can be divided into two classes based on the involved length scale: atomic and macroscopic. Atomic-scale effects are connected with the irregularities of the crystal lattice such as the interfaces, particular elements distribution in alloys [37], charged defects [38], etc. The magnitude of these effects is still the subject of investigation; the atomistic simulations based on the tight-binding method [39] predict considerably larger values than those relying on the empirical pseudopotential method [40]. In general, atomic-scale effects are weak compared to those on macroscale. For example, the magnitudes of about 1 μeV are reported for a specific alloy distribution in the AlGaAs barrier [37] of GaAs QDs. The effect is more pronounced when the dot material is an alloy, which should therefore be avoided when aiming at low FSS. A lower bound of several μeV was predicted for strain-tuned FSS in ternary $In_{0.6}Ga_{0.4}As$ QDs [41]. By macroscopic scale we mean for the purpose of the foregoing discussion that the characteristic length of the effect is comparable with the dimensions of a QD and the underlying crystal lattice is perceived as a homogeneous environment. Thus, the crystal symmetry is no longer relevant and the finite

*vlastimil.krapek@ceitec.vutbr.cz

values of FSS are now related to the symmetry lower than C_4, i.e., to the lateral elongation of the wave functions (e.g., envelope functions of the $\mathbf{k}\cdot\mathbf{p}$ theory). Principal contributions to the FSS on macroscopic scale arise from the asymmetric (elongated) shape of a QD and piezoelectric field. Further, it is possible to use the external strain field to induce the anisotropic effective mass tensor and modify the elongation of the hole wave functions and the related value of FSS [24].

Further information is contained in the polarization properties of the exciton doublet. Simple considerations assuming a purely heavy-hole exciton in an elliptic-disk-shaped QD [6] predicted a linear polarization of both transitions with the low-energy component polarized parallel with the long QD axis and the high-energy component having the orthogonal polarization. Typically, both structural-elongation and piezoelectric axes are parallel with the crystal axes [110] and $[1\bar{1}0]$, and so are the polarizations of both components. However, in some structures with shallow irregular confinement potential, such as quantum well thickness fluctuations, stochastic polarization directions were observed [5]. Further, when the light-hole contribution to the exciton ground state becomes important, the polarization orthogonality of both components is lost [24,42]. Thus, the definition of FSS as the difference between the exciton emission energies at [110] and $[1\bar{1}0]$ is not always correct, although it is widely used [14,20].

We focus here on QDs with type-II confinement, in which one type of charge carrier is confined in QD volume and the other in the barrier close to the QD vicinity. Possible inner/outer material combinations leading to the type-II confinement include InAs/GaAsSb and InP/GaInP with electrons bound in the inner material, and InP/GaP, GaSb/GaAs, or Ge/Si with holes bound in the inner material. In II-VI core/shell nanocrystals, electrons are confined in the core for CdTe/CdSe and holes for ZnSe/CdTe material combination [43]. The characteristic properties of type-II QDs are often discussed in the context of future applications. The radiative lifetime of excitations is tunable and can reach values considerably larger than in type I [44,45], which is exploited in QD flash memories [46,47]. In solar cells, QDs are used to enhance the infrared spectral response; the type-II QDs allow for an easier charge extraction due to their larger electron-hole separation [48,49].

The energies of excitons and excitonic complexes in type-II QDs have been frequently studied experimentally [50–54] and theoretically [55–63]. Those works focused on the energy scale above several meV (such as transition or binding energies). The excitonic FSS in type-II QDs has not been addressed so far.

The particular system of interest is InAs QDs with a thin $GaAs_{1-y}Sb_y$ overlayer embedded in GaAs [64–81]. One reason for selecting this material system is the possibility to induce a smooth crossover between type-I and type-II confinement regimes simply by changing y; the crossover values between 0.14 and 0.18 have been reported [65–67]. The other is that it belongs to systems with *holes* bound outside. Owing to their large effective mass the holes are more susceptible to the local potential profile or external perturbations, offering a larger potential for tuning their wave functions and the related FSS. The photoluminescence of $GaAs_{1-y}Sb_y$ capped QDs is rather intense [68,69] despite the type-II confinement with the radiative lifetimes as low as 10 ns [70,71]. The strain-reducing effect of the $GaAs_{1-y}Sb_y$ layer together with the surfacting effect of antimony allow one to increase the emission wavelengths of standard InAs QDs and reach the telecommunication wavelengths of 1.3 and 1.55 μm [72–74]. Various shapes of $GaAs_{1-y}Sb_y$ QDs have been reported, including a lens [75,76,82] or a pyramid with a graded In concentration [77]. Notably, the hole wave function is expected to be composed of two segments localized in the minima of the piezoelectric potential [66].

In this work we present a theoretical study of excitonic fine structure splitting of InAs QDs with $GaAs_{1-y}Sb_y$ overlayer. We propose a method to tune the FSS by setting the thickness of the $GaAs_{1-y}Sb_y$ layer. The values comparable with the natural linewidth can be achieved. The paper is organized as follows: In Sec. II a theory of FSS is described. To gain a qualitative understanding of the relations between the wave functions and FSS we discuss in Sec. III a simplified single-band model with Gaussian wave functions. The full calculations are presented in Sec. IV. We summarize and conclude in Sec. V.

II. THEORY

The single-particle states were calculated within the eight-band $\mathbf{k}\cdot\mathbf{p}$ theory [83,84], in which the wave functions are expanded into products of periodic parts of Bloch functions u_b in the Γ point and corresponding envelope functions χ_b,

$$\psi(\mathbf{r}) = \sum_{b\in\{x,y,z,s\}\otimes\{\uparrow,\downarrow\}} u_b(\mathbf{r})\chi_b(\mathbf{r}). \tag{1}$$

In this equation b is the band index, the bands x, y, z correspond to the valence band Bloch waves which are antisymmetric with respect to the corresponding mirror plane, and s corresponds to the conduction band Bloch wave. Following usual conventions, z denotes the growth direction. The calculations include the effects of the elastic strain via the Pikus-Bir Hamiltonian [85] and the piezoelectric field. The numeric simulations were performed with Nextnano 3D [86], which employs the finite difference method. The simulation space was discretized with a step of 1 nm. Material parameters were taken from the Nextnano database and they are also listed in the Supplementary material of Ref. [66].

Once the single-particle states are calculated, it is convenient to use them as a basis for the exciton state $|X\rangle$. First the Slater determinants $|X(ci,vj)\rangle = c^\dagger_{ci}c_{vj}|0\rangle$ are formed, where $|0\rangle$ is Fermi vacuum state (empty quantum dot), $c^\dagger_{ci}$ creates an electron in the ith conduction state, and c_{vj} annihilates an electron in the jth valence state; the corresponding single-particle wave functions are denoted ψ_{ci} and ψ_{vj}, respectively. For the calculations of FSS we used four Slater determinants formed from the ground hole and electron states. Following Ref. [6] [Eq. (2.3)] the exciton Hamiltonian matrix elements read

$$\begin{aligned}&\langle X(ci,vj)|\hat{H}|X(ck,vl)\rangle\\ &\quad = (E_i - E_j)\delta_{ik}\delta_{jl} + C(ci,vj,ck,vl) + EX(ci,vj,ck,vl),\end{aligned}$$

where E_i is the energy of the ith single-particle state, C represents the direct Coulomb interaction, and EX represents the exchange interaction.

Defining

$$S_{c,v}(\mathbf{r}) = \sum_{b\in\{s,x,y,z\}\otimes\{\uparrow,\downarrow\}} \chi^*_{c,b}(\mathbf{r})\chi_{v,b}(\mathbf{r})$$

and vector $\mathbf{T}$ with the components

$$T^x_{c,v}(\mathbf{r}) = \frac{P}{E_g}\sum_{\sigma\in\uparrow,\downarrow}[\chi^*_{c,s\sigma}(\mathbf{r})\chi_{v,x\sigma}(\mathbf{r}) + \chi^*_{c,x\sigma}(\mathbf{r})\chi_{v,s\sigma}(\mathbf{r})]$$

and T^y, T^z defined analogously (E_g is the fundamental band gap and P is one of the Kane's parameters related to the nonvanishing coordinate matrix elements $\langle x|x|s\rangle = P/E_g$), we can write

$$C(c1,v1;c2,v2) = -\frac{e^2}{4\pi\varepsilon}\int d\mathbf{r}_1\int d\mathbf{r}_2\frac{1}{|\mathbf{r}_1-\mathbf{r}_2|} \times S_{c1,c2}(\mathbf{r}_1)S_{v2,v1}(\mathbf{r}_2)$$

(e denotes the elementary charge and ε the dielectric function). The exchange Coulomb interaction term EX can be expressed as a sum of the following three terms:

$$EX_0(c1,v1;c2,v2) = \frac{e^2}{4\pi\varepsilon}\int d\mathbf{r}_1\int d\mathbf{r}_2\frac{1}{|\mathbf{r}_{12}|}S_{c1,v1}(\mathbf{r}_1)S_{v2,c2}(\mathbf{r}_2), \quad (2)$$

$$EX_1(c1,v1;c2,v2) = \frac{e^2}{4\pi\varepsilon}\int d\mathbf{r}_1\int d\mathbf{r}_2\frac{1}{|\mathbf{r}_{12}|^3}\mathbf{r}_{12}\cdot[S_{v2,c2}(\mathbf{r}_2)\mathbf{T}_{c1,v1}(\mathbf{r}_1) - S_{c1,v1}(\mathbf{r}_1)\mathbf{T}_{v2,c2}(\mathbf{r}_2)], \quad (3)$$

and

$$EX_2(c1,v1;c2,v2) = \frac{e^2}{4\pi\varepsilon}\int d\mathbf{r}_1\int d\mathbf{r}_2\frac{1}{|\mathbf{r}_{12}|^5}\sum_{\alpha,\beta\in x,y,z}\sum T^{(\alpha)}_{c1,v1}(\mathbf{r}_1)T^{(\beta)}_{v2,c2}(\mathbf{r}_2) \times\left[\delta_{\alpha\beta}|\mathbf{r}_{12}|^2 - 3r^\alpha_{12}r^\beta_{12}\right], \quad (4)$$

where $\mathbf{r}_{12} = \mathbf{r}_1 - \mathbf{r}_2$ and $\delta_{\alpha\beta}$ is the Kronecker delta. We note that S is nonzero only when the mixing of valence and conduction bands is taken into account. Thus, only the third term of the multipole expansion, Eq. (4), contributes to the FSS when this mixing is neglected, e.g., when single-band or six-band [87] $\mathbf{k}\cdot\mathbf{p}$ theory is used to obtain the wave function of individual particles. However, as the scaling of the terms with the linear extension of the wave function L goes as $EX_0 \sim 1/L$, $EX_1 \sim 1/L^2$, $EX_2 \sim 1/L^3$, the low-order terms are important, in particular, in larger QDs.

III. MODEL OF GAUSSIAN WAVE FUNCTIONS

Before treating realistic quantum dots with the full-complexity model, it is worth providing an intuitive understanding of the relation between the shape of the excitonic wave function and the value of FSS. To this end we employed a simplified model with the exciton composed of a single Slater determinant, no band mixing, and the electron and hole densities having the form of three-dimensional Gaussian functions. The electron and hole envelope functions read

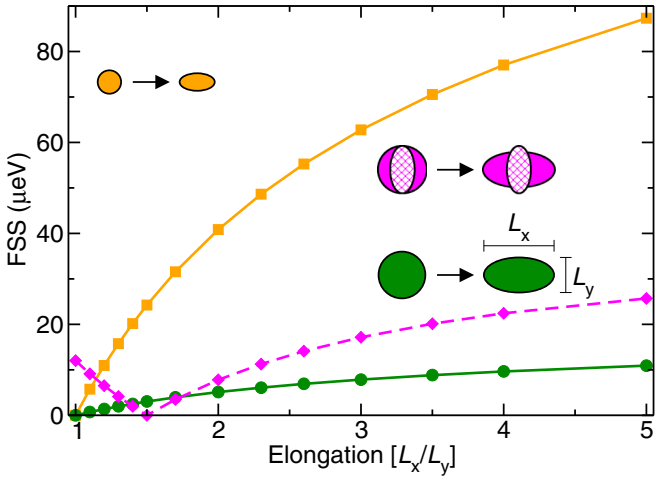

FIG. 1. (Color online) FSS as a function of the lateral elongation of the wave functions, defined as $E_w = L_x/L_y$. Orange line: A smaller dot with the extension parameters $L_x \times L_y = 25$ nm^2, $L_z = 2$ nm. The lateral extensions are varied preserving the value of their product (and thus the volume and vertical aspect ratio of a QD). Electron and hole wave functions have the same extensions and are elongated equally. Green line: A larger dot with the extensions twice larger than for the smaller dot, i.e., $L_x \times L_y = 100$ nm^2, $L_z = 4$ nm. Magenta line: A smaller dot, $L_x \times L_y = 25$ nm^2, $L_z = 2$ nm, with opposite electron and hole elongation. For electrons, E_w has a constant value of 2/3. For holes, E_w is varied and FSS is displayed as a function of the hole elongation. Insets: The insets schematically depict the wave functions. Hatched magenta ellipses correspond to the electron wave functions.

(normalization constant omitted for simplicity)

$$\chi_{e,h}(\mathbf{r}) \propto \sqrt{\exp\left[-\frac{(x-x_0)^2}{L_x^2} - \frac{(y-y_0)^2}{L_y^2} - \frac{(z-z_0)^2}{L_z^2}\right]},$$

where $L_{x,y,z}$ determine the spatial extensions of a particle and x_0, y_0, z_0 are the coordinates of its center. As the band mixing is neglected in the model, only the dipole-dipole exchange term [Eq. (4)] contributes to the FSS.

A crucial parameter for FSS is the lateral elongation of the envelope functions defined as $E_w = L_x/L_y$. It follows directly from Eq. (4) that for nonelongated envelope functions ($L_x = L_y$) FSS acquires a zero value. The dependence of the FSS on the elongation is shown in Fig. 1. In order to isolate the effect of the elongation and avoid unintentional variation of other parameters, we preserved the volume and the effective vertical aspect ratio of the model dots, i.e, values of L_z and the product $L_x \times L_y$ were kept constant. First, we assumed the same envelope function for both electrons and holes (orange and green lines). Such case corresponds, e.g., to strain-free GaAs/AlGaAs dots [88]. FSS exhibits a monotonically increasing concave dependence on the lateral elongation E_w. To demonstrate the effect of the QD volume, we show FSS for a smaller dot (extension parameters $L_x \times L_y = 25$ nm^2, $L_z = 2$ nm) and a larger dot with two-times larger dimensions (e.g., eight-times larger volume). The values of FSS for a larger QD are exactly eight times smaller. The inverse proportionality of FSS to the QD volume or to the third power of a characteristic linear dimension L can be directly inferred from Eq. (4).

With the band mixing taken into account, additional terms proportional to $1/L$ and $1/L^2$ emerge. However, the $1/L^3$ or $1/V$ scaling law (V representing a volume of the QD) has been recently demonstrated experimentally in realistic strain-free GaAs/AlGaAs QDs [15]. FSS values exceed the natural linewidth of the exciton recombination lines (up to units of μeV) even for a modest elongation. For example, for $E_w = 1.2$ we predict FSS of 11 μeV (1.4 μeV) in the smaller (larger) QD. We note that for the QDs studied in Ref. [15] we found the values of $L_x \times L_y$ between 11 and 36 nm^2 and L_z between 1 and 2 nm. The smaller dot case thus corresponds well to realistic GaAs/AlGaAs QDs.

Next, we introduce an important concept of the compensated elongation. For a suitable exciton wave function shape, FSS can attain a zero value even in the system that lacks the required symmetry C_{4v}. We consider the electron envelope function to be elongated in the direction perpendicular to the elongation of the hole envelope function, $E_{we} = 2/3$ (the subscripts e and h are used, when required, to distinguish the parameters of electrons and holes, respectively). The extension parameters correspond to the smaller dot: $L_x \times L_y = 25$ nm^2, $L_z = 2$ nm. FSS is plotted as a function of the hole elongation $E_{wh} \geqslant 1$ in Fig. 1 (magenta line). The prominent feature of the dependence is the zero-value minimum at $E_{wh} = 3/2$ (i.e., the inverse of the electron elongation. Intuitively, this can be described as the mutual compensation of both electron and hole elongations. The integral in Eq. (4) attains a zero value, which is, however, not related to the symmetry. In realistic QDs, the condition of the inverse elongation does not hold (due to band mixing or different volume of the envelope function of electrons and holes) but the effect is preserved. The minimum value of FSS can be larger than zero in case of QDs with the irregular shape. The effect of the compensated elongation has already been demonstrated experimentally utilizing the anisotropic external strain to vary the elongation of the hole envelope function [24]. In the following we will demonstrate that the elongation of the hole envelope function can be efficiently varied in type-II InAs QDs with GaAsSb capping layer.

The transition between type-I and type-II confinement in $GaAs_{1-y}Sb_y$ capped QDs is accompanied by the splitting of the hole wave function into two segments [66], evenly spread along the central electron wave function in QDs with a sufficient symmetry [Figs. 6(b) and 6(c)]. The behavior of FSS under such transition is shown in Fig. 2. When the segments are shifted from the central position along their long axis (orange line), small shifts effectively enhance the hole elongation and consequently the FSS. For larger shifts the wave function disintegrates; now the effect of increased distance of electron and hole prevails resulting into a decrease of FSS. The same behavior is predicted for nonelongated wave functions (green line), where the FSS dependence starts at a zero value, increases as the holes become effectively elongated, and decreases when the separation effects prevail. When the segments are shifted along their short axis, the effective elongation of the holes decreases as the segments are separated, and so happens with FSS. Depending on the magnitude of the original elongation, two possibilities exist: (1) The hole eventually becomes elongated in opposite direction (magenta line; note the magenta insets of Fig. 2 schematically depicting the change in the elongation direction). FSS goes through a zero value and starts to increase again. Finally, the separation effects prevail and FSS decreases. (2) When the original elongation is large, the hole disintegrates before the elongation direction is changed (maroon line). In such case a monotonously decreasing dependence of FSS on the segment distance is observed, governed first by the decrease of the effective elongation and then by the separation effects.

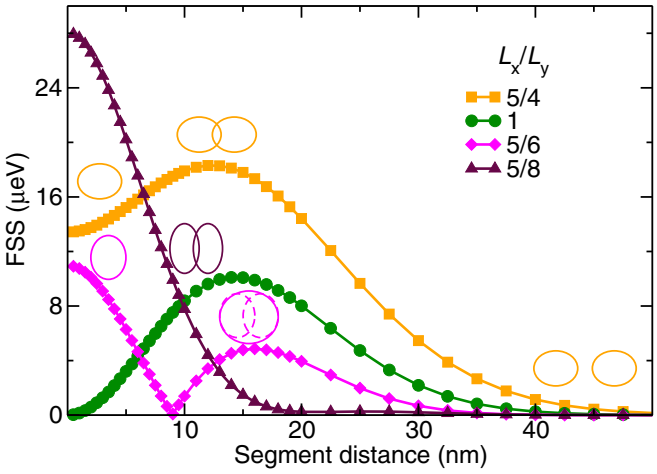

FIG. 2. (Color online) FSS for a hole wave function composed of two segments. The extensions of both electron and hole wave functions fulfill $L_x \times L_y = 25$ nm^2, $L_z = 2$ nm, with the lateral elongation $E_w = L_x/L_y$ of 5/4 (orange line, squares), 1 (green line, circles), 5/6 (magenta line, diamonds), and 5/8 (maroon line, triangles). The electron wave function is composed of a single Gaussian ($x_0 = 0$) while the hole wave function is split along x into two identical Gaussian segments evenly positioned around the central electron wave function ($x_0 = \pm d/2$, d being the segment distance). FSS is plotted as a function of the distance between the centers of the segments. Insets schematically depict the position and shape of the segments.

In strongly asymmetric QDs the minima in confinement potential corresponding to both segments can differ considerably and a single-segment hole wave function displaced from the central electron wave function can be formed. In such case there is no effective change in the elongation and the separation effect leads to a monotonous decrease of FSS (not shown).

IV. REALISTIC QUANTUM DOTS

We will now focus on realistic InAs QDs with a $GaAs_{1-y}Sb_y$ capping layer. We will show that FSS in such structures can be tuned by the thickness of the $GaAs_{1-y}Sb_y$ layer. Three QD geometries will be considered here, denoted as pyramidal, symmetric lens shaped, and elongated lens shaped. The *pyramidal* QD is adopted from Ref. [77] and has the shape of a pyramid with the base length of 22 nm, height of 8 nm, and the trumpet indium composition profile within the pyramid (see Ref. [77] for details). For the other structures we assume QDs composed of pure InAs. The *symmetric lens-shaped* QD motivated by Refs. [75,82] is modeled as a top of a sphere with the base radius of 8 nm and the height of 4 nm. A prominent form of the lateral asymmetry of QDs is their structural elongation. So far no elongation was reported for InAs QDs

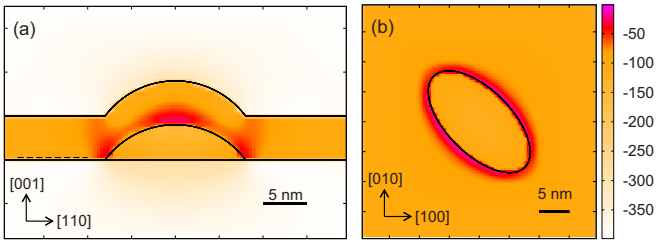

FIG. 3. (Color online) *Effective* confinement potential (color bar scale in meV) without the contribution of the piezoelectric field for holes in the *lens-shaped* QD. (a) $E_s = 1$, plane $(1\bar{1}0)$ through the QD center; (b) $E_s = 2$, plane (001) just above the QD base [the vertical position is shown in panel (a) by a dashed line]. Boundaries between different materials are schematically depicted. The potential is given from the electron view; the holes are confined near the largest values represented by the red/orange spots.

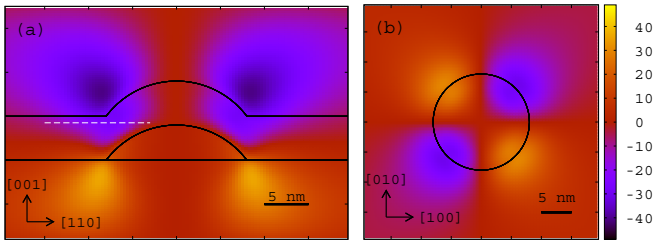

FIG. 4. (Color online) Piezoelectric potential (color bar scale in meV) for the *symmetric lens-shaped* QD. (a) plane $(1\bar{1}0)$ through the QD center; (b) plane (001) just above the top of the QD [i.e., above the horizontal nodal plane; the vertical position is shown in panel (a) by a white dashed line].

with $GaAs_{1-y}Sb_y$ overlayer, which is in striking contrast with InAs QDs capped by pure GaAs [89,90]. This can be attributed to the surfacting effect of antimony but it is also possible that the elongation has been overlooked as the methods involved in experimental studies were insensitive to it. Therefore, we consider in our study also the possibility that QDs are elongated. In accordance with GaAs capped InAs QDs [90,91] we select the direction $[1\bar{1}0]$ as the main elongation axis and quantify the elongation by the ratio of characteristic lateral dimensions along $[1\bar{1}0]$ and [110], denoted as E_s in the following (the subscript s is used to differentiate the structural elongation from the wave-function elongation used in the previous section). The *elongated lens-shaped* QDs are formed from the lens-shaped dot by its stretching along $[1\bar{1}0]$ and compressing along [110] by the same factor so that the QD volume and height are preserved; the radii for $E_s = 2$ read 11.3 and 5.65 nm, etc. All QDs are capped with the $GaAs_{0.8}Sb_{0.2}$ layer of a certain thickness and further embedded in GaAs. Our choice of the Sb content is similar to the values reported in experiments [71,77,78] and was motivated by its proximity to the crossover between the type-I and type-II confinement which allows one to adjust the type of confinement by selecting a proper thickness of the $GaAs_{1-y}Sb_y$ layer.

The shape of the wave functions is closely connected with the confinement potential, which is contributed by the band-edge offsets, strain field, and piezoelectric potential. Here, we visualize the confinement by the *effective* potential constructed from the eigenvalues of the pointwise diagonalized Hamiltonian (terms containing the spatial derivatives are discarded and the Hamiltonian is then diagonalized at each point of the simulation grid). In contrast with the standard confinement potential entering the Schrödinger equation, the *effective* potential involves the strain-induced band mixing.

The hole *effective* potentials in all type-II QDs discussed further in the paper exhibit qualitatively similar features. We will present them for the *lens-shaped* QD with the GaAsSb layer thickness of 5 nm and with the elongation E_s of either 1 or 2. Figure 3 shows the potential profile without the piezoelectric contribution. The potential is given from the electron view; the largest values correspond to the minima of the hole confinement. Zero energy is set to the valence band edge of bulk unstrained InAs. Two local minima of the hole confinement potential are formed in the GaAsSb layer along the sides of the QD and above its top [Fig. 3(a)]. The top minimum is of the light-hole character and therefore penalized by the quantum confinement. The ground hole state will be localized in the side minimum which forms a ring around the QD [Fig. 3(b)], in which weak variations of the potential are present with two rather shallow absolute minima along the long QD side (i.e., in [110] direction from the QD center). Depending on the magnitude of these variations, the wave function might form a ring or be split into two segments.

The piezoelectric field has an octopole shape, shown in Fig. 4. Its contribution is rather important as its magnitude of about 50 meV is comparable to the variations of the rest of the confinement potential inside the $GaAs_{1-y}Sb_y$ layer. The horizontal nodal plane of the piezoelectric octopole lies close to the side minimum of the confinement potential. The piezoelectric potential therefore tends to split the wave function of the holes in the side minimum into two segments situated along [110] below the nodal plane or along $[1\bar{1}0]$ above the nodal plane.

The total *effective* confinement potential is shown in Fig. 5. The following shapes of the hole wave function are possible: (i) inside a QD (type I), (ii) a ringlike shape along the QD when the piezoelectric field is too weak to localize the holes in its minima, (iii) two segments at the dot base situated along [110] [Figs. 5(a) and 5(c)], and (iv) two segments at the QD sides above the piezoelectric nodal plane situated along $[1\bar{1}0]$ due to the piezoelectric field [Fig. 5(b)] or along [110] when the structural elongation along $[1\bar{1}0]$ prevails [Fig. 5(d) is close to that case]. In pyramidal QDs with the trumpet In composition profile, both the side minimum of the confinement potential and the piezoelectric octopole are shifted up towards the region of large In content. In short, there is a rich variety of the hole wave-function shapes. Variation of the parameters such as the thickness or the composition of the GaAsSb layer are supposed to induce transitions between those shapes. For example, switching between the deep narrow minima below the nodal plane [Figs. 5(a) and 5(c)] and shallow broad minima above the nodal plane [Figs. 5(b) and 5(d)] shall be achievable. Considering the effect of the compensated elongation, this results in nontrivial dependences of FSS on structural parameters and opens an interesting prospect for the tuning of FSS.

Figure 6(d) shows the dependence of FSS on the thickness of the $GaAs_{1-y}Sb_y$ layer in two *lens-shaped* QDs: *symmetric*

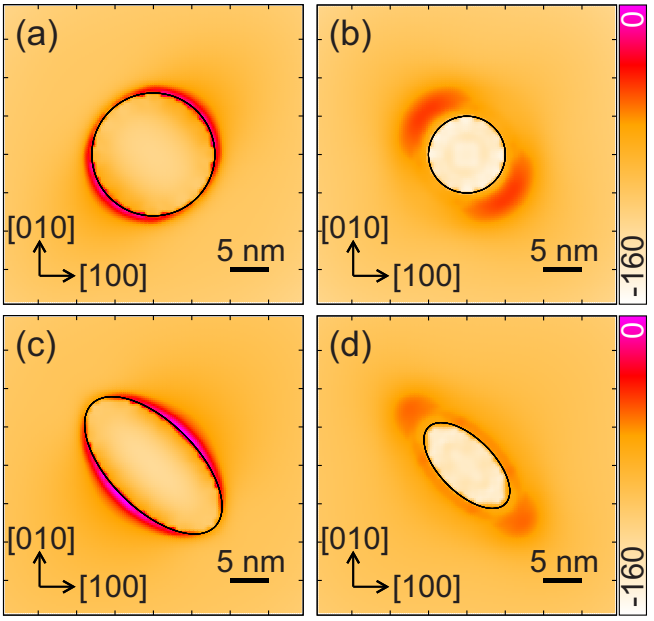

FIG. 5. (Color online) Total *effective* confinement potential (color bar scale in meV) including the contribution of the piezoelectric field for holes in the *lens-shaped* QD. (a), (c) Plane (001) below the nodal plane of the piezoelectric potential (just above the QD base), $E_s = 1$ (a) and 2 (c). (b), (d) Plane (001) above the nodal plane of the piezoelectric potential (3 nm above the QD base), $E_s = 1$ (b) and 2 (d). Black circles and ellipses display the QD boundary at respective heights. The potential is given from the electron view; the holes are confined near the largest values represented by the red/orange spots.

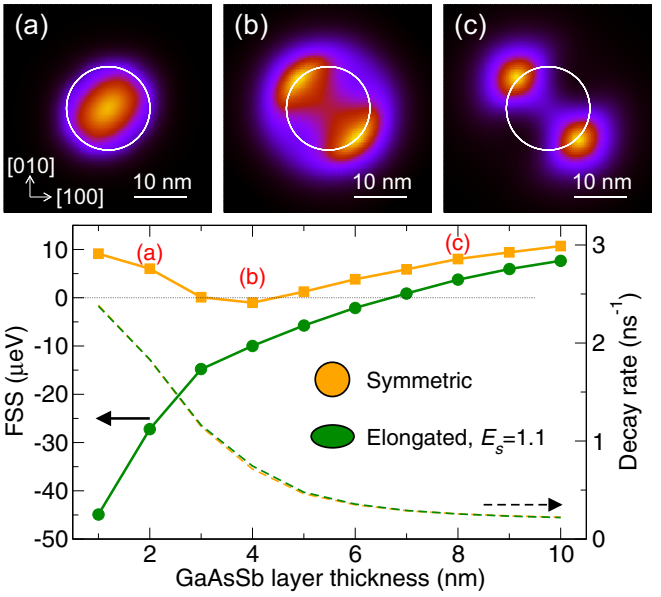

FIG. 6. (Color online) (a)–(c) Planar probability density of the hole ground state in the *symmetric lens-shaped* QD (height 4 nm, radius 8 nm), plane (001) (integrated over [001]) for the $GaAs_{0.8}Sb_{0.2}$ layer thickness of (a) 2 nm, (b) 4 nm, and (c) 8 cm. The QD boundary at the base height is displayed with the white line. (d) FSS (thick solid lines with symbols, left) and exciton radiative decay rate (thin dashed lines) between the ground electron and hole state in the *symmetric lens-shaped* QD (orange) and the *elongated lens-shaped* QD with $E_s = 1.1$ (green) as functions of the GaAsSb layer thickness. The polarization of the lower exciton component is encoded into the sign of FSS: positive/negative sign corresponds to the polarization along $[110]/[1\bar{1}0]$, respectively. The red labels denote the points corresponding to the maps of the probability density.

and weakly elongated ($E_s = 1.1$). We exploit the fact that the excitons in our model exhibit only two well-defined polarizations and encode the polarization of the lower exciton component into the sign of the FSS. In this way, the level crossing is better visible. We will first discuss the case of the symmetric QD. The electron wave function is weakly elongated in the $[1\bar{1}0]$ direction and as it resides within the QD, its variation with the thickness of the $GaAs_{1-y}Sb_y$ layer is negligible. For a thin $GaAs_{1-y}Sb_y$ layer (up to 3 nm) the ground hole wave function resides inside the QD, too. It experiences the bottom part of the piezoelectric octopole and is thus elongated in [110], as shown in Fig. 6(a). The polarization of the lower exciton component is [110]. With increasing thickness a hole ground state gradually shifts into the $GaAs_{1-y}Sb_y$ layer and also slightly upwards (for about 1.3 nm for the full range of thicknesses). Consequently, it becomes split by the upper part of the piezoelectric octopole into two segments along $[1\bar{1}0]$. For the thickness interval between 3 and 5 nm, the segmented wave function behaves as effectively elongated in $[1\bar{1}0]$ [Fig. 6(b)] and the lower exciton component is also polarized along $[1\bar{1}0]$. For the thickness values above 5 nm, the segments are well separated and the elongation of each segment in [110] determines the character of the wave function. The lower exciton component is again polarized along [110]. Thus, we distinguish three regions of different exciton polarization. At each of the two transitions between those regions, exciton levels cross and FSS is reduced to zero. We note that minimum values obtained in our calculations are nonzero due to the finite step in the thickness dependence and read 0.1 and 1 μeV for the first and second transition, respectively. The observed behavior of FSS corresponds well to the qualitative prediction of the model of Gaussian function for $L_x/L_y = 5/6$ (cf. Fig. 2, magenta line).

Similar behavior is observed in a lens-shaped QD weakly elongated in $[1\bar{1}0]$ [Fig. 6(d), green lines]. The first region is now missing, as the elongation of the hole wave function within the QD volume (for a thin $GaAs_{1-y}Sb_y$ layer) is now $[1\bar{1}0]$ because the structural elongation dominates over the piezoelectric contribution. The zero FSS is reached for a $GaAs_{1-y}Sb_y$ layer thickness of 7 nm. Figure 7 shows the FSS dependence on the thickness of the $GaAs_{1-y}Sb_y$ layer in a *pyramidal* QD with the trumpet profile (height of 8 nm and base size of 22 nm). As in the case of the lens-shaped QDs, the hole wave function changes its effective elongation during the crossover between the type-I and type-II confinement and in turn, exciton levels cross and FSS is reduced towards zero. Thus, variations of the $GaAs_{1-y}Sb_y$ layer thickness present a universal approach to tune and reduce FSS. For a typical lifetime of InAs QDs of 1 ns, the natural linewidth of the exciton recombination is 4 μeV; experimentally predicted spectral linewidth approaches 100 μeV [92]. Both values are larger than the minimum accessible values predicted here for the $GaAs_{1-y}Sb_y$ capped QDs.

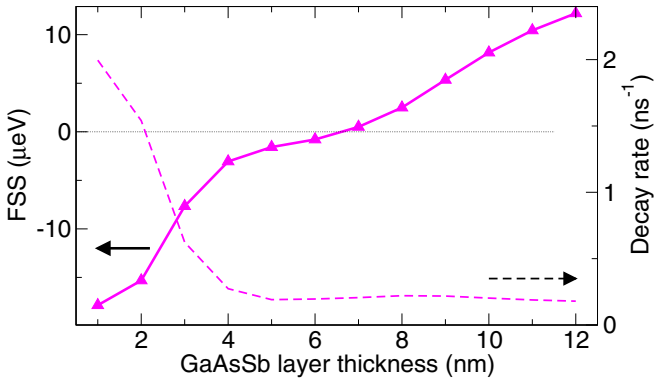

FIG. 7. (Color online) FSS (thick solid line with symbols, left) and exciton radiative decay rate (thin dashed line) between the ground electron and hole state in the pyramid-shaped QD as functions of the GaAsSb layer thickness. The polarization of the lower exciton component is encoded into the sign of FSS: positive/negative sign corresponds to the polarization along [110]/[1$\bar{1}$0], respectively.

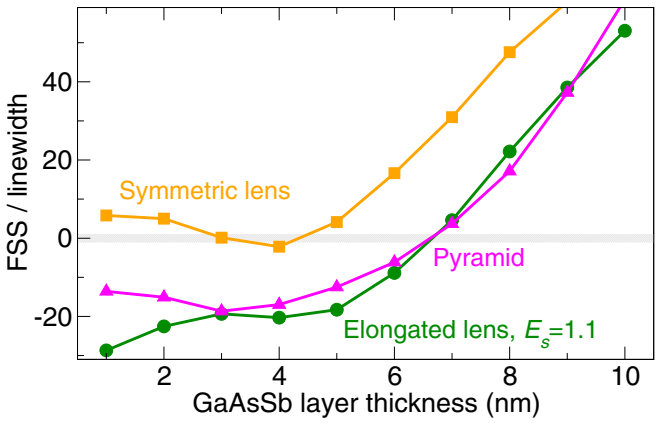

FIG. 8. (Color online) FSS divided by the natural spectral linewidth of exciton transitions between the ground electron and hole state in the *symmetric lens-shaped* QD (orange), the *elongated lens-shaped* QD with $E_s = 1.1$ (green), and the *pyramid-shaped* QD (magenta) as functions of the GaAsSb layer thickness. The polarization of the lower exciton component is encoded into the sign of FSS: positive/negative sign corresponds to the polarization along [110]/[1$\bar{1}$0], respectively.

We note that due to the idealized QD shapes considered in the study the exciton levels exhibit crossing, i.e., FSS goes through zero and the polarizations of the transitions are changed abruptly. In realistic QDs, which are always somewhat irregular, exciton levels undergo anticrossing with a nonzero minimum FSS and smooth polarization variations. We do not address this issue here as no experimental data related to the irregularities is available. The interested reader is referred to a detailed discussion [93] and studies of different QD systems [24,37].

Finally we argue that $GaAs_{1-y}Sb_y$ capped InAs QDs can be good emitters even in the type-II confinement regime. There is experimental evidence of intense photoluminescence from the $GaAs_{1-y}Sb_y$ capped InAs QDs [70], about four times weaker than for the reference type-I sample and about three times stronger after rapid thermal annealing. Roughly 15-times higher exciton lifetime has been reported (0.7 ns in type I compared to 11.2 ns in type II) [70]. We support these observations with the calculations of the exciton radiative decay rate γ_R shown in Figs. 6(d) and 7. The radiative exciton lifetime $\tau_R = \gamma_R^{-1}$ reads [94]

$$\tau_R^{-1} = \frac{e^2 n_r E_X}{\pi m_0^2 \varepsilon_0 \hbar^2 c^3} \sum_{\mathbf{e}} |\langle 0|\mathbf{e}\cdot\hat{\mathbf{p}}|X\rangle|^2,$$

where e is the elementary charge, n_r is the refractive index (a square root of the relative permittivity given in Ref. [66]), E_X is the exciton energy, m_0 is the free electron mass, $\hbar$ is the Planck constant, c is the speed of light, $|X\rangle$ and $|0\rangle$ denote the exciton and vacuum wave function, respectively, $\hat{\mathbf{p}}$ is the momentum operator, $\mathbf{e}$ is the polarization vector, and the summation goes over three independent polarizations. Typical calculated lifetimes for type-I QDs are in the range 0.4–0.5 ns. The values corresponding to the minima of FSS are 0.9 and 2.2 ns for the *symmetric lens-shaped* QD, 3.4 ns for the *elongated lens-shaped* QD, and 4.8 ns for the *pyramidal* QD. The comparison with the experimental values suggests that the theoretical values might be somewhat underestimated but the trends shall be reproduced. Thus, roughly twice to ten-times higher exciton lifetime as compared to type-I QDs is expected. For this reason we are convinced that the extraction of individual photons from individual $GaAs_{1-y}Sb_y$ capped QDs will be experimentally feasible.

The natural linewidth of the exciton transitions is $\hbar/\tau_R$. The increase of the lifetime in type-II structures therefore results in narrower transitions. For the generation of entangled photon pairs the FSS needs to be compared with the spectral linewidth. The FSS divided by the spectral linewidth for all previously considered QDs is shown in Fig. 8. The gray-shaded rectangle highlights the area of quasidegenerate exciton transitions (with the FSS lower than the spectral width), in which the generation of the entangled photon pairs is possible. As the area is rather narrow, a postgrowth selection of QDs or further tuning might be required to produce the polarization-entangled photon pairs.

V. CONCLUSIONS

In $GaAs_{1-y}Sb_y$ capped InAs QDs, lateral symmetry of the hole wave functions can be to a large extent influenced by the thickness of the $GaAs_{1-y}Sb_y$ layer. In particular, during the crossover between type-I and type-II confinement regimes, the hole wave function is shifted upwards across the nodal plane of the piezoelectric octopole, which is accompanied by the change of the direction of lateral elongation. Due to the mechanism of compensated elongation, a crossing of the bright exciton levels and a reduction of FSS to zero is predicted for certain thicknesses of the $GaAs_{1-y}Sb_y$ layer. Low natural FSS and efficient photoluminescence make the $GaAs_{1-y}Sb_y$ capped InAs QDs attractive as a possible source of entangled photon pairs.

ACKNOWLEDGMENTS

This work was supported by European Social Fund (Grant No. CZ.1.07/2.3.00/30.0005), European Regional Development Fund (Project No. CZ.1.05/1.1.00/02.0068),

Czech Science Foundation (Grant No. 15-21581S), Technology Agency of the Czech Republic (Grant No. TE01020233), and EU 7th Framework Programme (Contracts No. 286154—SYLICA and No. 280566—UnivSEM). P.K. was supported by the internal project MUNI/A/1496/2014.

[1] D. Gammon, E. S. Snow, B. V. Shanabrook, D. S. Katzer, and D. Park, Phys. Rev. Lett. **76**, 3005 (1996).
[2] M. Bayer, G. Ortner, O. Stern, A. Kuther, A. A. Gorbunov, A. Forchel, P. Hawrylak, S. Fafard, K. Hinzer, T. L. Reinecke *et al.*, Phys. Rev. B **65**, 195315 (2002).
[3] D. Kovalev, H. Heckler, G. Polisski, and F. Koch, Phys. Status Solidi B **215**, 871 (1999).
[4] V. D. Kulakovskii, G. Bacher, R. Weigand, T. Kümmell, A. Forchel, E. Borovitskaya, K. Leonardi, and D. Hommel, Phys. Rev. Lett. **82**, 1780 (1999).
[5] J. D. Plumhof, V. Křápek, L. Wang, A. Schliwa, D. Bimberg, A. Rastelli, and O. G. Schmidt, Phys. Rev. B **81**, 121309 (2010).
[6] T. Takagahara, Phys. Rev. B **62**, 16840 (2000).
[7] N. I. Cade, H. Gotoh, H. Kamada, H. Nakano, and H. Okamoto, Phys. Rev. B **73**, 115322 (2006).
[8] M. E. Ware, E. A. Stinaff, D. Gammon, M. F. Doty, A. S. Bracker, D. Gershoni, V. L. Korenev, S. C. Bădescu, Y. Lyanda-Geller, and T. L. Reinecke, Phys. Rev. Lett. **95**, 177403 (2005).
[9] M. Kroutvar, Y. Ducommun, D. Heiss, M. Bichler, D. Schuh, G. Abstreiter, and J. J. Finley, Nature (London) **432**, 81 (2004).
[10] T. Takagahara, Phys. Rev. B **60**, 2638 (1999).
[11] W. Langbein, R. Zimmermann, E. Runge, and J. Hvam, Phys. Status Solidi B **221**, 349 (2000).
[12] N. Accanto, F. Masia, I. Moreels, Z. Hens, W. Langbein, and P. Borri, ACS Nano **6**, 5227 (2012).
[13] F. Masia, N. Accanto, W. Langbein, and P. Borri, Phys. Rev. Lett. **108**, 087401 (2012).
[14] R. Seguin, A. Schliwa, S. Rodt, K. Pötschke, U. W. Pohl, and D. Bimberg, Phys. Rev. Lett. **95**, 257402 (2005).
[15] Y. H. Huo, V. Křápek, A. Rastelli, and O. G. Schmidt, Phys. Rev. B **90**, 041304 (2014).
[16] O. Benson, C. Santori, M. Pelton, and Y. Yamamoto, Phys. Rev. Lett. **84**, 2513 (2000).
[17] A. Schliwa, M. Winkelnkemper, A. Lochmann, E. Stock, and D. Bimberg, Phys. Rev. B **80**, 161307 (2009).
[18] M. Abbarchi, C. A. Mastrandrea, T. Kuroda, T. Mano, K. Sakoda, N. Koguchi, S. Sanguinetti, A. Vinattieri, and M. Gurioli, Phys. Rev. B **78**, 125321 (2008).
[19] W. Langbein, P. Borri, U. Woggon, V. Stavarache, D. Reuter, and A. D. Wieck, Phys. Rev. B **69**, 161301 (2004).
[20] R. J. Young, R. M. Stevenson, A. J. Shields, P. Atkinson, K. Cooper, D. A. Ritchie, K. M. Groom, A. I. Tartakovskii, and M. S. Skolnick, Phys. Rev. B **72**, 113305 (2005).
[21] B. D. Gerardot, S. Seidl, P. A. Dalgarno, R. J. Warburton, D. Granados, J. M. García, K. Kowalik, O. Krebs, K. Karrai, A. Badolato *et al.*, Appl. Phys. Lett. **90**, 041101 (2007).
[22] M. M. Vogel, S. M. Ulrich, R. Hafenbrak, P. Michler, L. Wang, A. Rastelli, and O. G. Schmidt, Appl. Phys. Lett. **91**, 051904 (2007).
[23] R. M. Stevenson, R. J. Young, P. See, D. G. Gevaux, K. Cooper, P. Atkinson, I. Farrer, D. A. Ritchie, and A. J. Shields, Phys. Rev. B **73**, 033306 (2006).
[24] J. D. Plumhof, V. Křápek, F. Ding, K. D. Jöns, R. Hafenbrak, P. Klenovský, A. Herklotz, K. Dörr, P. Michler, A. Rastelli *et al.*, Phys. Rev. B **83**, 121302 (2011).
[25] A. Rastelli, F. Ding, J. D. Plumhof, S. Kumar, R. Trotta, C. Deneke, A. Malachias, P. Atkinson, E. Zallo, T. Zander *et al.*, Phys. Status Solidi B **249**, 687 (2012).
[26] R. Trotta, E. Zallo, C. Ortix, P. Atkinson, J. D. Plumhof, J. van den Brink, A. Rastelli, and O. G. Schmidt, Phys. Rev. Lett. **109**, 147401 (2012).
[27] N. Akopian, N. H. Lindner, E. Poem, Y. Berlatzky, J. Avron, D. Gershoni, B. D. Gerardot, and P. M. Petroff, Phys. Rev. Lett. **96**, 130501 (2006).
[28] M. Ghali, K. Ohtani, Y. Ohno, and H. Ohno, Nat. Commun. **3**, 661 (2012).
[29] M. A. M. Versteegh, M. E. Reimer, K. D. Jöns, D. Dalacu, P. J. Poole, A. Gulinatti, A. Giudice, and V. Zwiller, Nat. Commun. **5**, 5298 (2014).
[30] T. Huber, A. Predojević, M. Khoshnegar, D. Dalacu, P. J. Poole, H. Majedi, and G. Weihs, Nano Lett. **14**, 7107 (2014).
[31] R. Trotta, J. S. Wildmann, E. Zallo, O. G. Schmidt, and A. Rastelli, Nano Lett. **14**, 3439 (2014).
[32] L. Sapienza, R. N. E. Malein, C. E. Kuklewicz, P. E. Kremer, K. Srinivasan, A. Griffiths, E. Clarke, M. Gong, R. J. Warburton, and B. D. Gerardot, Phys. Rev. B **88**, 155330 (2013).
[33] X. Liu, N. Ha, H. Nakajima, T. Mano, T. Kuroda, B. Urbaszek, H. Kumano, I. Suemune, Y. Sakuma, and K. Sakoda, Phys. Rev. B **90**, 081301 (2014).
[34] E. Goldmann, S. Barthel, M. Florian, K. Schuh, and F. Jahnke, Appl. Phys. Lett. **103**, 242102 (2013).
[35] A. I. Tartakovskii, M. N. Makhonin, I. R. Sellers, J. Cahill, A. D. Andreev, D. M. Whittaker, J.-P. R. Wells, A. M. Fox, D. J. Mowbray, M. S. Skolnick *et al.*, Phys. Rev. B **70**, 193303 (2004).
[36] A. I. Tartakovskii, R. S. Kolodka, H. Y. Liu, M. A. Migliorato, M. Hopkinson, M. N. Makhonin, D. J. Mowbray, and M. S. Skolnick, Appl. Phys. Lett. **88**, 131115 (2006).
[37] J.-W. Luo, R. Singh, A. Zunger, and G. Bester, Phys. Rev. B **86**, 161302 (2012).
[38] R. Singh and G. Bester, Phys. Rev. B **85**, 205405 (2012).
[39] M. Zieliński, Phys. Rev. B **88**, 155319 (2013).
[40] R. Singh and G. Bester, Phys. Rev. B **84**, 241402 (2011).
[41] R. Singh and G. Bester, Phys. Rev. Lett. **104**, 196803 (2010).
[42] J. D. Plumhof, R. Trotta, V. Křápek, E. Zallo, P. Atkinson, S. Kumar, A. Rastelli, and O. G. Schmidt, Phys. Rev. B **87**, 075311 (2013).
[43] S. Kim, B. Fisher, H.-J. Eisler, and M. Bawendi, J. Am. Chem. Soc. **125**, 11466 (2003).
[44] Y. Jang, T. Badcock, D. Mowbray, M. Skolnick, J. Park, D. Lee, H. Liu, M. Steer, and M. Hopkinson, Appl. Phys. Lett. **92**, 251905 (2008).
[45] L. P. Balet, S. A. Ivanov, A. Piryatinski, M. Achermann, and V. I. Klimov, Nano Lett. **4**, 1485 (2004).

[46] A. Marent, M. Geller, A. Schliwa, D. Feise, K. Pötschke, D. Bimberg, N. Akçay, and N. Öncan, Appl. Phys. Lett. **91**, 242109 (2007).

[47] M. Geller, A. Marent, T. Nowozin, D. Bimberg, N. Akçay, and N. Öncan, Appl. Phys. Lett. **92**, 092108 (2008).

[48] R. Laghumavarapu, A. Moscho, A. Khoshakhlagh, M. El-Emawy, L. Lester, and D. Huffaker, Appl. Phys. Lett. **90**, 173125 (2007).

[49] S. Itzhakov, H. Shen, S. Buhbut, H. Lin, and D. Oron, J. Phys. Chem. C **117**, 22203 (2013).

[50] K. Matsuda, S. V. Nair, H. E. Ruda, Y. Sugimoto, T. Saiki, and K. Yamaguchi, Appl. Phys. Lett. **90**, 013101 (2007).

[51] M. Nakaema, F. Iikawa, M. Brasil, E. Ribeiro, G. Medeiros-Ribeiro, W. Carvalho, Jr., M. Maialle, and M. Degani, Appl. Phys. Lett. **81**, 2743 (2002).

[52] M. Hayne, J. Maes, S. Bersier, V. V. Moshchalkov, A. Schliwa, L. Müller-Kirsch, C. Kapteyn, R. Heitz, and D. Bimberg, Appl. Phys. Lett. **82**, 4355 (2003).

[53] F. Iikawa, M. P. F. Godoy, M. K. K. Nakaema, M. J. S. P. Brasil, M. Z. Maialle, M. A. Degani, E. Ribeiro, G. Medeiros-Ribeiro, W. Carvalho, Jr., and J. A. Brum, Braz. J. Phys. **34**, 555 (2004).

[54] P. Klenovský, M. Brehm, V. Křápek, E. Lausecker, D. Munzar, F. Hackl, H. Steiner, T. Fromherz, G. Bauer, and J. Humlíček, Phys. Rev. B **86**, 115305 (2012).

[55] J. M. Rorison, Phys. Rev. B **48**, 4643 (1993).

[56] P. Lelong, K. Suzuki, G. Bastard, H. Sakaki, and Y. Arakawa, Physica E **7**, 393 (2000).

[57] K. L. Janssens, B. Partoens, and F. M. Peeters, Phys. Rev. B **66**, 075314 (2002).

[58] K. L. Janssens, B. Partoens, and F. M. Peeters, Phys. Rev. B **67**, 235325 (2003).

[59] M. P. F. de Godoy, P. F. Gomes, M. K. K. Nakaema, F. Iikawa, M. J. S. P. Brasil, R. A. Caetano, J. R. Madureira, J. R. R. Bortoleto, M. A. Cotta, E. Ribeiro *et al.*, Phys. Rev. B **73**, 033309 (2006).

[60] V. Mlinar, M. Tadić, and F. M. Peeters, Phys. Rev. B **73**, 235336 (2006).

[61] J. R. Madureira, M. P. de Godoy, M. Brasil, and F. Iikawa, Appl. Phys. Lett. **90**, 212105 (2007).

[62] A. Piryatinski, S. A. Ivanov, S. Tretiak, and V. I. Klimov, Nano Lett. **7**, 108 (2007).

[63] J. M. Miloszewski, S. Tomić, and D. Binks, J. Phys.: Conf. Ser. **526**, 012005 (2014).

[64] K. Akahane, N. Yamamoto, and N. Ohtani, Physica E **21**, 295 (2004).

[65] H. Y. Liu, M. J. Steer, T. J. Badcock, D. J. Mowbray, M. S. Skolnick, F. Suarez, J. S. Ng, M. Hopkinson, and J. P. R. David, J. Appl. Phys. **99**, 046104 (2006).

[66] P. Klenovský, V. Křápek, D. Munzar, and J. Humlíček, Appl. Phys. Lett. **97**, 203107 (2010).

[67] P. Klenovský, V. Křápek, D. Munzar, and J. Humlíček, J. Phys.: Conf. Ser. **245**, 012086 (2010).

[68] K. Akahane, N. Yamamoto, S. Gozu, and N. Ohtani, Physica E **26**, 395 (2005).

[69] H. Y. Liu, M. J. Steer, T. J. Badcock, D. J. Mowbray, M. S. Skolnick, P. Navaretti, K. M. Groom, M. Hopkinson, and R. A. Hogg, Appl. Phys. Lett. **86**, 143108 (2005).

[70] J. M. Ulloa, J. M. Llorens, B. Alén, D. F. Reyes, D. L. Sales, D. González, and A. Hierro, Appl. Phys. Lett. **101**, 253112 (2012).

[71] W.-S. Liu, H.-L. Tseng, and P.-C. Kuo, Opt. Express **22**, 18860 (2014).

[72] J. M. Ripalda, D. Granados, Y. González, A. M. Sánchez, S. I. Molina, and J. M. García, Appl. Phys. Lett. **87**, 202108 (2005).

[73] A. Hospodková, E. Hulicius, J. Pangrác, J. Oswald, J. Vyskočil, K. Kuldová, T. Šimeček, P. Hazdra, and O. Caha, J. Cryst. Growth **312**, 1383 (2010).

[74] M. Zíková, A. Hospodková, J. Pangrác, J. Oswald, P. Krčil, E. Hulicius, P. Komninou, and J. Kioseoglou, J. Cryst. Growth **414**, 167 (2015).

[75] W.-T. Hsu, Y.-A. Liao, F.-C. Hsu, P.-C. Chiu, J.-I. Chyi, and W.-H. Chang, Appl. Phys. Lett. **99**, 073108 (2011).

[76] A. Hospodková, J. Pangrác, J. Vyskočil, M. Zíková, J. Oswald, P. Komninou, and E. Hulicius, J. Cryst. Growth **414**, 156 (2015).

[77] J. M. Ulloa, I. W. D. Drouzas, P. M. Koenraad, D. J. Mowbray, M. J. Steer, H. Y. Liu, and M. Hopkinson, Appl. Phys. Lett. **90**, 213105 (2007).

[78] C. Y. Jin, H. Y. Liu, S. Y. Zhang, Q. Jiang, S. L. Liew, M. Hopkinson, T. J. Badcock, E. Nabavi, and D. J. Mowbray, Appl. Phys. Lett. **91**, 021102 (2007).

[79] J. M. Ulloa, R. Gargallo-Caballero, M. Bozkurt, M. del Moral, A. Guzmán, P. M. Koenraad, and A. Hierro, Phys. Rev. B **81**, 165305 (2010).

[80] K. Gradkowski, T. J. Ochalski, N. Pavarelli, H. Y. Liu, J. Tatebayashi, D. P. Williams, D. J. Mowbray, G. Huyet, and D. L. Huffaker, Phys. Rev. B **85**, 035432 (2012).

[81] A. Hospodková, M. Zíková, J. Pangrác, J. Oswald, K. Kuldová, J. Vyskočil, and E. Hulicius, J. Cryst. Growth **370**, 303 (2013).

[82] A. Hospodková, M. Zíková, J. Pangrác, J. Oswald, J. Kubištová, K. Kuldová, P. Hazdra, and E. Hulicius, J. Phys. D: Appl. Phys. **46**, 095103 (2013).

[83] G. Bastard, Phys. Rev. B **24**, 5693 (1981).

[84] O. Stier, M. Grundmann, and D. Bimberg, Phys. Rev. B **59**, 5688 (1999).

[85] G. E. Pikus and G. L. Bir, Sov. Phys. Solid State **1**, 1502 (1960).

[86] S. Birner, T. Zibold, T. Andlauer, T. Kubis, M. Sabathil, A. Trellakis, and P. Vogl, IEEE Trans. Electron Dev. **54**, 2137 (2007).

[87] J. M. Luttinger and W. Kohn, Phys. Rev. **97**, 869 (1955).

[88] L. Wang, V. Křápek, F. Ding, F. Horton, A. Schliwa, D. Bimberg, A. Rastelli, and O. G. Schmidt, Phys. Rev. B **80**, 085309 (2009).

[89] V. Křápek, K. Kuldová, J. Oswald, A. Hospodková, E. Hulicius, and J. Humlíček, Appl. Phys. Lett. **89**, 153108 (2006).

[90] K. Kuldová, V. Křápek, A. Hospodková, O. B. Zrzavecká, J. Oswald, E. Hulicius, and J. Humlíček, Mater. Sci. Eng. C **26**, 983 (2006).

[91] R. Songmuang, S. Kiravittaya, and O. Schmidt, J. Cryst. Growth **249**, 416 (2003).

[92] J. Skiba-Szymanska, A. Jamil, I. Farrer, M. B. Ward, C. A. Nicoll, D. J. P. Ellis, J. P. Griffiths, D. Anderson, G. A. C. Jones, D. A. Ritchie *et al.*, Nanotechnology **22**, 065302 (2011).

[93] J. D. Plumhof, R. Trotta, A. Rastelli, and O. G. Schmidt, Nanoscale Res. Lett. **7**, 336 (2012).

[94] M. Sugawara, Phys. Rev. B **51**, 10743 (1995).